

Quantum transport of topological spin solitons in a one-dimensional organic ferroelectric


S. Imajo^{1,*}, A. Miyake¹, R. Kurihara¹, M. Tokunaga¹, K. Kindo¹, S. Horiuchi², and F. Kagawa^{3,4}

¹*Institute for Solid State Physics, University of Tokyo, Kashiwa, Chiba 277-8581, Japan*

²*Research Institute of Advanced Electronics and Photonics (RIAEP), National Institute of Advanced Industrial Science and Technology (AIST), Tsukuba 305-8565, Japan*

³*RIKEN Center for Emergent Matter Science (CEMS), Wako 351-0198, Japan*

⁴*Department of Applied Physics, University of Tokyo, Tokyo 113-8656, Japan*

 (Received 25 November 2020; revised 5 March 2021; accepted 12 May 2021; published 21 May 2021)

We report the dielectric, magnetic, and ultrasonic properties of a one-dimensional organic salt TTF-QBr₃I. These indicate that TTF-QBr₃I shows a ferroelectric spin-Peierls (FSP) state in a quantum critical regime. In the FSP state, coupling of charge, spin, and lattice leads to emergent excitation of spin solitons as topological defects. Amazingly, the solitons are highly mobile even at low temperatures, although they are normally stationary because of pinning. Our results suggest that strong quantum fluctuations enhanced near a quantum critical point enable soliton motion governed by athermal relaxation. This indicates the realization of quantum topological transport at ambient pressure.

DOI: [10.1103/PhysRevB.103.L201117](https://doi.org/10.1103/PhysRevB.103.L201117)

One-dimensional systems exhibit a rich variety of physics related to lattice instabilities through coupling with charge and/or spin degrees of freedom. The entanglement of multiple degrees of freedom provides intriguing phases and exotic excitations. One representative example is the spin-Peierls (SP) transition which induces lattice deformation triggered by spin-singlet dimerization. Whereas this transition has been extensively examined in long-standing theories [1–3], its experimental realization is still limited to only a handful of one-dimensional materials, such as CuGeO₃ [4], NaV₂O₅ [5], and some organic compounds [6–9]. Among them, one-dimensional organic charge-transfer complexes have received particular attention because of the strong lattice-charge/spin coupling in molecular crystals. MEM(TCNQ)₂ (MEM=N-methyl-N-ethylmorpholinium, TCNQ=7,7',8,8'-tetracyanoquinodimethane) [6], TTF-AuS₄C₄(CF₃)₄ (TTF=tetrathiafulvalene) [7,8], (TMTTF)₂PF₆ (TMTTF=tetramethyltetrathiafulvalene) [9], etc. have been investigated as model systems and have provided significant information on the SP transition, such as the high-field incommensurate phase [8] and pressure-induced quantum criticality [9]. TTF-QBr₄ (QBr₄ denotes *p*-bromanil) is also known to undergo the SP transition at 53 K [10–13]. However, this salt is quite unique because it is the only example that the SP transition occurs simultaneously with a paraelectric-ferroelectric transition [10–14]. TTF-QBr₃I (2-iodo-3,5,6-tri-bromo-*p*-benzoquinone) focused in this study is isomorphous with TTF-QBr₄ although this transition has not been observed [15]. In these salts, the charge transfer between the donor (D=TTF) and acceptor (A = QBr₄ or QBr₃I) makes these molecules fully ionic, D⁺ and A[−], in the whole temperature range [10–12]. This means that

TTF-QBr₄ and TTF-QBr₃I are regarded as one-dimensional ionic Mott insulators [14]. Note that the crystal structure and electronic state of these salts are distinct from those of the other well-known nonmagnetic ferroelectrics, TTF-QCl₄ [16–20], TTF-QBrCl₃ [21], and TTF-QBr₂I₂ [15,22], which exhibits the neutral-ionic (N-I) transition instead of the SP transition. This difference manifests in magnetism and electrical conductivity, as discussed in Ref. [14].

As displayed in Fig. 1(a), D⁺ and A[−] are alternately stacked in a one-dimensional chain in TTF-QBr₄ and TTF-QBr₃I. At room temperature, the uniform stacking without long-range dimerization provides the paraelectric paramagnetic state [Fig. 1(b)]. Once the SP transition occurs, the static dimerization alters the paramagnetic state into a nonmagnetic state. The static displacement of D⁺ and A[−] simultaneously leads to ferroelectric order along the chains. The coupling of the dielectric and magnetic transitions opens up a novel route for magnetic-field-controllable ferroelectrics [12]. From another viewpoint of the ferroelectric SP (FSP) state, domain formation should be noted because two patterns of opposite dimerization are degenerate, as illustrated by patterns 1 and 2 in Fig. 1(c). The two patterns coexist by forming domains, and consequently, domain walls (DWs) are created at their border. In the case of the N-I ferroelectric systems [15–22], some excitations, such as a polaron, a N-I DW, a spin soliton, and a charge soliton, have been discussed in terms of topological defects. On the other hand, in the fully ionic FSP state, only the spin soliton is hosted as the DW as presented in Fig. 1(d). This means that we can discuss the pure contribution of the spin soliton, which should be intriguing in terms of topological spin excitation; however, the presence of spin solitons in the FSP state has not yet been observed. Moreover, the jump of the polarization at the DWs endows the spin solitons with bound charge [23], and therefore, dynamics of the spin soliton can organize topological transport of spin and charge. In this

*imajo@issp.u-tokyo.ac.jp

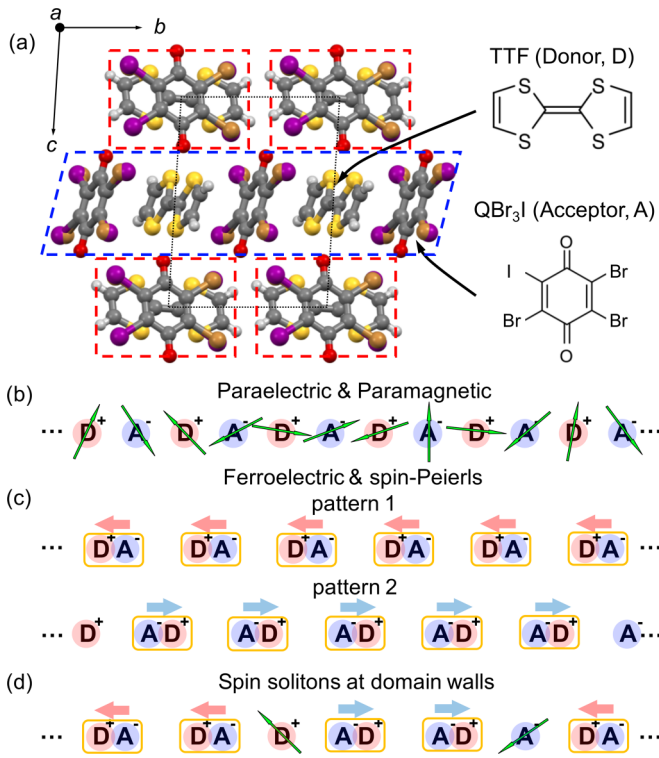


FIG. 1. (a) Crystal structure viewed along the a axis, and chemical forms of TTF and QBr_3I molecules. The dashed boxes signify the one-dimensional chains along the a axis (red) and b axis (blue). [(b) and (c)] Schematic illustrations of the arrangement of the D^+ and A^- molecules in (b) the paraelectric paramagnetic state and (c) the FSP state. The green arrows represent the magnetic spin. The red and blue arrows signify the directions of the electric dipoles in the D^+A^- dimers. In the FSP state shown in (c), two degenerate patterns occur, patterns 1 and 2, according to the direction of the dipole moments. (d) Creation of spin solitons at the ferroelectric DWs in the FSP state.

work, we examine the dielectric, magnetic, and ultrasonic properties of $\text{TTF-QBr}_3\text{I}$ to discuss the low-temperature emergent phenomena produced by the coupling of charge, spin, and lattice degrees of freedom in a one-dimensional system. We first discover the FSP state occurring in the quantum critical region. As expected in the one-dimensional FSP system, the presence of solitonic spins created at the DWs is detected. Moreover, athermal relaxation between the potential minima of the energy landscape manifests in the low-temperature dynamics due to the strong quantum fluctuations. These results promise realization of quantum transport of the topological spins in $\text{TTF-QBr}_3\text{I}$ at ambient pressure.

First, to discuss the low-temperature state of $\text{TTF-QBr}_3\text{I}$ from the perspective of the dielectric response, we present the temperature dependence of the dielectric permittivity in Fig. 2(a). At 4–5 K ($=T_{\text{FSP}}$), the permittivity exhibits an anomaly. Below 5 K, the permittivity shows the frequency dependence (see Fig. S1 in Ref. [24]), which may arise from the ferroelectric domain dynamics as in the case of other ferroelectrics [15,17,22]. The frequency-dependent behavior makes the determination of T_{FSP} difficult, but indicates that the macroscopic ferroelectric domains should be formed above 5 K. The behavior seems to be different from that of

typical ferroelectrics such as TTF-QBr_4 , but, it strongly resembles that of ferroelectricity in the quantum critical regime (quantum ferroelectricity) [15]. This implies that quantum fluctuations influence the ferroelectricity. We therefore evaluate the temperature dependence of the permittivity above 10 K by using the Barrett formula for quantum paraelectricity [30]:

$$\epsilon_r(T) = C/[(T_1/2)\coth(T_1/2T) - T_0] + A, \quad (1)$$

where T_0 and T_1 denote the classical Curie-Weiss temperature and the crossover temperature from the classical regime to the quantum-mechanical regime. The obtained parameters are $T_0 \sim 4$ K and $T_1 \sim 60$ K. The positive value of T_0 directly indicates the presence of a ferroelectric interaction. In addition, the quantum effect on the ferroelectricity is expected to be strong because the ratio between T_0 and T_1 reaches 15, which is much larger than that of other quantum paraelectrics [31,32]. To assess whether the ferroelectricity of $\text{TTF-QBr}_3\text{I}$ is in the quantum critical region, the reciprocal permittivity $1/\epsilon_r$ is displayed in Fig. 2(b). In quantum ferroelectrics, $1/\epsilon_r$ varies as T^2 [15,33,34], in contrast to the Curie-Weiss behavior $1/\epsilon_r \sim T$ in classical ferroelectrics. $\text{TTF-QBr}_3\text{I}$ exhibits the quantum critical behavior $1/\epsilon_r \sim T^2$, distinct from the $1/\epsilon_r \sim T$ dependence for classical ferroelectrics such as TTF-QBr_4 in Fig. 2(c). The dielectric response above 5 K in $\text{TTF-QBr}_3\text{I}$ is governed by the strongly developed quantum fluctuations of the FSP state. Namely, the chemical substitution from TTF-QBr_4 to $\text{TTF-QBr}_3\text{I}$ shifts the ferroelectric transition toward the brink of the quantum critical point (QCP). Indeed, the low-temperature ϵ_r of $\text{TTF-QBr}_3\text{I}$ is enhanced by the quantum criticality— ϵ_r of $\text{TTF-QBr}_3\text{I}$ becomes twice larger than that of TTF-QBr_4 at 5 K.

Next, to confirm the excitation of spin solitons, we display the magnetization curve at 4.2 K in Fig. 2(d). By simply decomposing the M - H curve, we obtain the noninteracting paramagnetic component described as the $S = 1/2$ Brillouin function ($\sim 7\%$) and the almost linear contribution. The former is considered to originate from spin solitons because the distance between the diluted spin solitons is sufficiently long to disregard the exchange interaction of the solitons [16,21]. Although it is hard to estimate the number of static impurity spins precisely, the main contribution of the paramagnetic component should be the spin solitons because the number of impurity spins is typically smaller than 1% in TTF-QX_4 salts [12,15,16,21] thanks to the unique molecular shape, which prevents the crystals from having defects and impurities. The heat capacity measurement also detects the noninteracting component as the two-level-type Schottky anomaly (see Fig. S2 [24]), and the value is almost consistent with the value $0.07\mu_B$. We should notice that this value is determined as a static average of the soliton density, which may differ in other time scales depending on the creation and annihilation speed of the solitons. The almost linear contribution should arise from the antiferromagnetically coupled spins in the TTF and QBr_3I chains. Even if the ferroelectric transition observed at ~ 5 K is accompanied by the SP transition, the almost linear behavior is reasonable because the transition temperature is quite close to the measurement temperature of 4.2 K. To clarify that the SP transition simultaneously appears at the same temperature of 4–5 K, in Fig. 2(e), we present the temperature dependence of the total and subtracted magnetic susceptibility

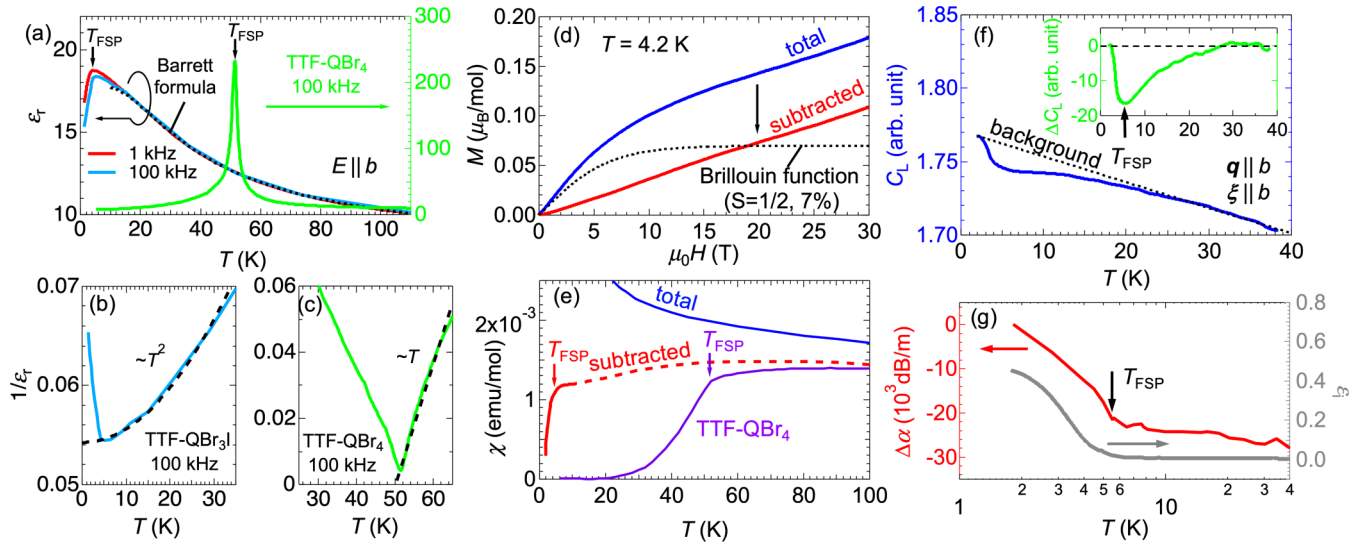


FIG. 2. (a) Temperature dependence of the dielectric permittivity in 1 kHz (red) and 100 kHz (light blue) ac electric fields. The reported data of TTF-QBr₄ (light green) are also shown on the right axis. The dotted curves are the fits to the Barrett formula with the parameters mentioned in the text. [(b) and (c)] $1/\epsilon_r$ vs T plot of TTF-QBr₃I data (b) and TTF-QBr₄ data (c) shown in (a). (d) Magnetization curves up to 30 T at 4.2 K. The blue curve represents the total magnetization of TTF-QBr₃I, while the red curve denotes the magnetization obtained by subtracting the paramagnetic component displayed by the dotted curve. (e) Total and subtracted magnetic susceptibility as a function of temperature. The susceptibility is obtained by subtracting the Curie-type paramagnetic component as mentioned in the text and Ref. [24]. Since the subtraction is valid only around 4.2 K, the higher-temperature data are shown as the dashed curve. The purple curve presents the data for TTF-QBr₄. The arrows signify the FSP transition temperatures. (f) Temperature dependence of the elastic constant for longitudinal ultrasonic waves along the b axis C_L . The dashed curve is a background curve estimated based on the normal elastic stiffening [35]. The inset displays the additional component related to the FSP transition derived by subtracting the background. (g) Relative change in temperature-dependent ultrasonic attenuation $\Delta\alpha$ plotted in a semilogarithmic plot. The data of imaginary part of the dielectric permittivity ϵ_i at 1 kHz are also shown on the right axis.

χ at 1 T after the soliton contribution estimated by the M - H curve has been subtracted. Note that the number of spin solitons should depend on temperature. Above the FSP transition, the number of spin solitons is smaller, but not zero, because local domain formation exists as a dimerization fluctuation as in the case of TTF-QBr₄ [12]. Although the accurate values of χ are between the subtracted and nonsubtracted data, the abrupt decrease of χ at low temperatures indicates that the transition temperature is almost 5 K. This behavior evidences the occurrence of the SP transition together with the ferroelectric transition, as in the case of TTF-QBr₄.

Based on the dielectric and magnetic measurement results, we confirm the FSP transition at ~ 5 K and the presence of spin solitons in TTF-QBr₃I. Since the transition originates from the one-dimensional lattice instability, we next investigate the ultrasonic properties sensitive to lattice deformation. Figures 2(f) and 2(g) show the elastic constant C_L and the relative change in the ultrasonic attenuation coefficient $\Delta\alpha$ for longitudinal ultrasonic waves as a function of temperature, respectively. C_L is known to increase with decreasing temperature due to the normal stiffening of the lattice [35], regarded as a background component, as denoted by the dashed line in Fig. 2(f). Thus, the additional component shown by the green curve in the inset should correspond to the phonon softening due to the FSP transition. The behavior indicates that fluctuating dimerization grows below 30 K in the high-temperature paramagnetic state as mentioned above and that the long-range dimerization of the SP transition occurs at 5–6 K [36]. In Fig. 2(g), the temperature dependence of $\Delta\alpha$ also shows

an anomaly coming from the FSP transition. Although $\Delta\alpha$ in the SP state usually decreases with decreasing temperature due to the formation of an energy gap [37], it increases below the transition temperature. This means that scattering of the acoustic phonons is enhanced in the FSP state. This behavior makes sense because the emergence of the domain structure increases the scattering rate at the domain boundaries. Indeed, this temperature dependence is quite similar to that of the imaginary part of the permittivity ϵ_i , which reflects energy dissipation by the domain dynamics in ac electric fields, as shown in Fig. 2(g). In other words, the scattering between the phonons and spin solitons is promoted with decreasing temperature in the FSP state, as a result of the strong lattice-spin coupling in the present material.

From our comprehensive investigations, we find that TTF-QBr₃I exhibits the FSP transition at ~ 5 K, clearly detected as dielectric, magnetic, and ultrasonic anomalies. Interestingly, the low-temperature transition occurs in the quantum critical region, in contrast to the high-temperature FSP transition for TTF-QBr₄. Considering the difference between the two systems, i.e., the halogen atoms Br and I, working as a chemical pressure [15], the negative chemical pressure thrusts the FSP transition into the quantum critical region, as illustrated in Fig. 3. Note that the effect of randomness originating from the replacement with asymmetric molecules on TTF-QX₄ is typically less significant than the chemical pressure according to the earlier reports for TTF-QBrCl₃ [21] and DM-TTF-QBr_nCl_{4-n} [38]. This pressure-controllable phase diagram agrees with the typical concept of the quantum criticality

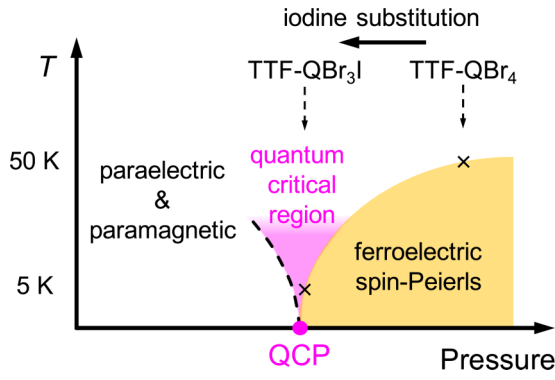


FIG. 3. Schematic illustration of the temperature-pressure phase diagram for the FSP system. TTF-QBr₃I is positioned in the quantum critical region located around the QCP.

for second-order transition between ordered and disordered phases. The degeneracy of the FSP ground states yields the domain structure, as detected by the augmentation of the ultrasonic attenuation. In the FSP state, the domains produce spin solitons at their boundaries as topological defects. To gain more insight into the FSP state in the quantum critical region, we further scrutinize the low-temperature permittivity in detail below. As shown in Fig. 2(a), the permittivity exhibits a frequency dependence at low temperatures. This behavior arises from the dynamics of the ferroelectric domains similar to those in other organic ferroelectrics [17,18,22]. This means that the frequency dependence induced by the DW dynamics directly reflects the soliton motion. The characteristic relaxation time τ can be derived by examining at the frequency dependence of the dielectric permittivity shown in Fig. 4(a). The behavior is well reproduced by one mode of the Cole-Cole-type relaxation shown in the figure [39], and from this analysis, we obtain τ as a function of inverse temperature shown in Fig. 4(b). The stretching parameter in the relaxation equation, α , is ~ 0.7 in this temperature region. The large value of α is consistent with the enhancement of α with approaching the ferroelectric QCP observed in other quantum ferroelectrics [22]. This means that the developed quantum fluctuations make the spectral width of the DW response broad. To shift a DW, recombination of the dimer is required, as is illustrated in Fig. 4(c). The energy for the dimer dissociation corresponds to the activation energy Δ , which acts as an effective pinning mechanism and results in the thermal activation behavior of the soliton motion. Thus, the relaxation time of the domain dynamics is exponentially suppressed with decreasing temperature. The linear dependence of τ below $\sim 0.4 \text{ K}^{-1}$ (above $\sim 2.5 \text{ K}$) in this plot exactly demonstrates the Arrhenius-type behavior of the dynamics, indicating slowing of the soliton motion towards low temperatures. However, surprisingly, the decrease in τ deviates from the linear dependence at low temperatures, $1/T > \sim 0.4 \text{ K}^{-1}$ (i.e., $T < \sim 2.5 \text{ K}$), and the fast relaxation ($\tau \sim 10^{-4} \text{ s}$) seems to survive even in the zero-temperature limit. This means that the spin solitons are highly mobile without suffering from pinning even at low temperatures, which is in marked contrast to the typical dynamic freezing of glasses described by the Vogel-Fulcher-Tammann equation [40]. Similar behavior has been

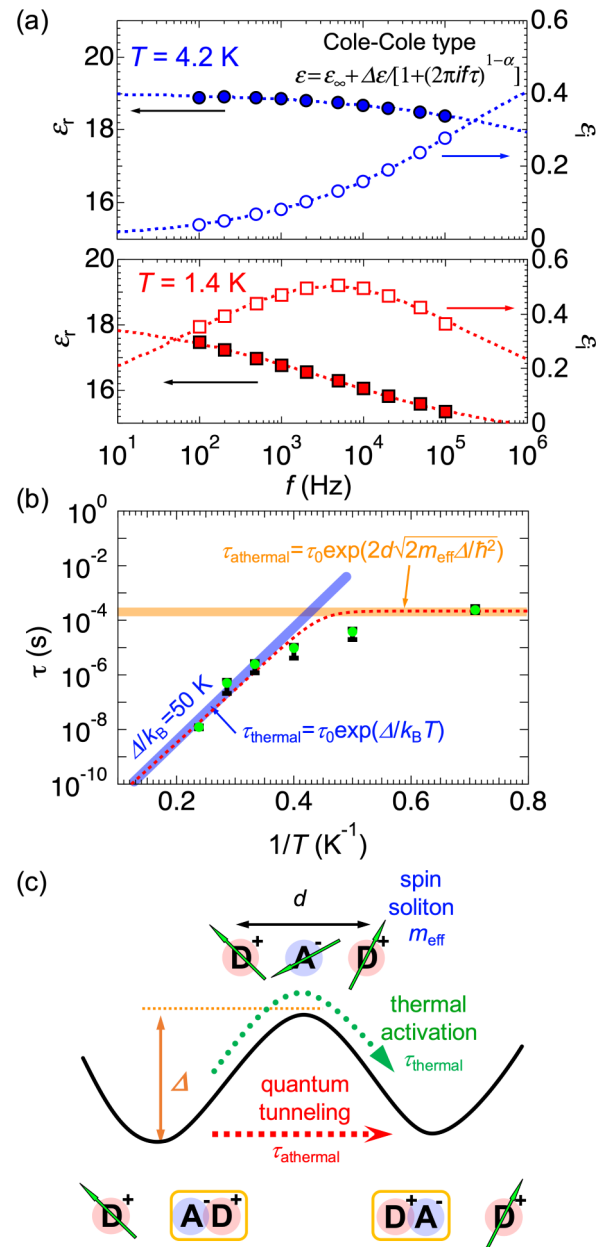


FIG. 4. (a) Permittivity-frequency profiles at 1.4 and 4.2 K. The dotted curves denote fits to the Cole-Cole type relaxation described in the figure. (b) Relaxation time as a function of inverse temperature. The blue line shows the Arrhenius-type linear dependence of the classical relaxation, whereas the orange line is the constant relaxation of the quantum tunneling. The dotted curve indicates a simple approximation of the crossover between the classical and quantum regime obtained by the Wentzel-Kramers-Brillouin model. (c) Schematic energy landscape describing the disassociation and recombination of the dimer accompanied by the annihilation and creation of spin solitons. The parameters d , Δ , and m_{eff} denote the unit cell distance, activation energy and effective mass of the spin solitons, respectively. τ_{athemal} and τ_{thermal} are the relaxation times of the quantum tunneling process and thermal activation process crossing the potential.

reported in the previous work on the quantum ferroelectric state of the ferroelectric N-I transition [22]. Those researchers concluded that the ferroelectric DWs creep in an athermal

process dominated by the quantum fluctuations enhanced near the QCP. Although the magnetic degree of freedom is quenched in the ferroelectric N-I transition because of the simultaneous charge transfer, the similar response indicates that the spin solitons in TTF-QBr₃I are also transmitted across the potential landscape by quantum tunneling. Thus, in the same manner, we evaluate the dynamics of the spin solitons with a simple model, the Wentzel-Kramers-Brillouin approximation [22,41] for quantum tunneling and Matthiessen's rule by the following formula:

$$\begin{aligned} \tau(T) &= (1/\tau_{\text{thermal}} + 1/\tau_{\text{athermal}})^{-1} \\ &= \tau_0 / [\exp(-\Delta/k_B T) + \exp(-2d\sqrt{2m_{\text{eff}}\Delta/\hbar^2})], \quad (2) \end{aligned}$$

where d signifies the tunneling distance of the soliton, namely, the unit cell length along the column, $\approx 8.5 \text{ \AA}$ [15], and m_{eff} represents the effective mass of the spin soliton. τ_0 is the attempt relaxation time. The first term τ_{thermal} represents the relaxation time of the Arrhenius-type relaxation, while the second term τ_{athermal} denotes that of the quantum relaxation. The behavior cannot be completely described by the present simple approximation depicted by the red dotted curve, but the assumption roughly gives some parameters related to the dynamics. The estimated values of m_{eff} and Δ/k_B are $\sim 1000m_e$ (m_e is the electron mass) and $\sim 50 \text{ K}$, respectively. These two are the origin of the fast τ_{athermal} . Since the tunneling of the spin solitons involves displacement of the molecules, m_{eff} should be on the order of the masses of TTF and QBr₃I (10^5m_e – 10^6m_e); however, the obtained m_{eff} is several hundred times smaller than the expected value. In earlier reports on

the soliton/DW dynamics [22,42], a similar drastic diminishment was observed and discussed from the viewpoint of the soliton width. The decrease in Δ when approaching the QCP causes broadening of the DW width with the development of quantum fluctuations. For TTF-QBr₄, the previous work [12] reported a spin gap value of $\Delta/k_B \sim 250 \text{ K}$, which should be comparable with Δ because both the gaps are the energy difference between the order and disorder states. The approach to the QCP certainly gives the much smaller $\Delta/k_B \sim 50 \text{ K}$ for TTF-QBr₃I, which reasonably reduces the effective mass by the strong broadening of the soliton width. Accordingly, the nearness to the QCP, giving the light m_{eff} and small Δ , entails the fast dynamics of the spin solitons, indicative of the quantum transport of the topological spin solitons.

The present results substantiate that the FSP state of TTF-QBr₃I is inside the quantum critical region. The topological spin solitons in the FSP state are endowed with high mobility even in the low-temperature region owing to the strengthened quantum fluctuations. The pure transport of the spin solitons induced by the quantum fluctuations must materialize in TTF-QBr₃I. This quantum transport is distinct from the DWs thermally traveling near a room-temperature critical point in the N-I ferroelectric salt TTF-QCl₄ [18–20]. Since this promises unique transport mediated by the flowing spin solitons, further studies, such as thermal transport measurements, are the interesting subjects for future work.

We thank Y. Nemoto and M. Akatsu (Niigata University) for supplying the LiNbO₃ piezoelectric transducers used in this study. This study was partly supported by JST CREST Grant No. JPMJCR18J2.

-
- [1] M. C. Cross and D. S. Fisher, *Phys. Rev. B* **19**, 402 (1979).
 [2] M. C. Cross, *Phys. Rev. B* **20**, 4606 (1979).
 [3] J. W. Bray, L. V. Interrante, I. S. Jacobs, and J. C. Bonner, *The Spin-Peierls Transition* (Springer, Boston, MA, 1983).
 [4] M. Hase, I. Terasaki, and K. Uchinokura, *Phys. Rev. Lett.* **70**, 3651 (1993).
 [5] M. Isobe and Y. Ueda, *J. Phys. Soc. Jpn.* **65**, 1178 (1996).
 [6] S. Huizinga, J. Kommandeur, G. A. Sawatzky, B. T. Thole, K. Kopinga, W. J. M. de Jonge, and J. Roos, *Phys. Rev. B* **19**, 4723 (1979).
 [7] I. S. Jacobs, J. W. Bray, H. R. Hart, Jr., L. V. Interrante, J. S. Kasper, G. D. Watkins, D. E. Prober, and J. C. Bonner, *Phys. Rev. B* **14**, 3036 (1976).
 [8] J. A. Northby, H. A. Groenendijk, L. J. de Jongh, J. C. Bonner, I. S. Jacobs, and L. V. Interrante, *Phys. Rev. B* **25**, 3215 (1982).
 [9] D. S. Chow, P. Wzietek, D. Fogliatti, B. Alavi, D. J. Tantillo, C. A. Merlic, and S. E. Brown, *Phys. Rev. Lett.* **81**, 3984 (1998).
 [10] A. Girlando, C. Pecile, and J. B. Torrance, *Solid State Commun.* **54**, 753 (1985).
 [11] Y. Tokura, S. Koshihara, Y. Iwasa, H. Okamoto, T. Komatsu, T. Koda, N. Iwasawa, and G. Saito, *Phys. Rev. Lett.* **63**, 2405 (1989).
 [12] F. Kagawa, S. Horiuchi, M. Tokunaga, J. Fujioka, and Y. Tokura, *Nat. Phys.* **6**, 169 (2010).
 [13] S. Horiuchi, K. Kobayashi, R. Kumai, and S. Ishibashi, *Chem. Lett.* **43**, 26 (2014).
 [14] K. Sunami, Y. Sakai, R. Takehara, H. Adachi, K. Miyagawa, S. Horiuchi, and K. Kanoda, *Phys. Rev. Res.* **2**, 043333 (2020).
 [15] S. Horiuchi, K. Kobayashi, R. Kumai, N. Minami, F. Kagawa, and Y. Tokura, *Nat. Commun.* **6**, 7469 (2015).
 [16] T. Mitani, G. Saito, Y. Tokura, and T. Koda, *Phys. Rev. Lett.* **53**, 842 (1984).
 [17] H. Okamoto, T. Mitani, Y. Tokura, S. Koshihara, T. Komatsu, Y. Iwasa, T. Koda, and G. Saito, *Phys. Rev. B* **43**, 8224 (1991).
 [18] K. Sunami, T. Nishikawa, K. Miyagawa, S. Horiuchi, R. Kato, T. Miyamoto, H. Okamoto, and K. Kanoda, *Sci. Adv.* **4**, eaau7725 (2018).
 [19] R. Takehara, K. Sunami, K. Miyagawa, T. Miyamoto, H. Okamoto, S. Horiuchi, R. Kato, and K. Kanoda, *Sci. Adv.* **5**, eaax8720 (2019).
 [20] R. Takehara, K. Sunami, F. Iwase, M. Hosoda, K. Miyagawa, T. Miyamoto, H. Okamoto, and K. Kanoda, *Phys. Rev. B* **98**, 054103 (2018).
 [21] F. Kagawa, S. Horiuchi, H. Matsui, R. Kumai, Y. Onose, T. Hasegawa, and Y. Tokura, *Phys. Rev. Lett.* **104**, 227602 (2010).
 [22] F. Kagawa, N. Minami, S. Horiuchi, and Y. Tokura, *Nat. Commun.* **7**, 10675 (2016).
 [23] P. S. Bednyakov, T. Sluka, A. K. Tagantsev, D. Damjanovic, and N. Setter, *Sci. Rep.* **5**, 15819 (2015).

- [24] See Supplemental Material at <http://link.aps.org/supplemental/10.1103/PhysRevB.103.L201117> for the detailed analyses of the present measurements and additional information, which includes Refs. [25–29].
- [25] J. Wosnitzer, X. Liu, D. Schweitzer, and H. J. Keller, *Phys. Rev. B* **50**, 12747 (1994).
- [26] S. Imajo, N. Kanda, S. Yamashita, H. Akutsu, Y. Nakazawa, H. Kumagai, T. Kobayashi, and A. Kawamoto, *J. Phys. Soc. Jpn.* **85**, 043705 (2016).
- [27] W. H. Korving, G. J. Kramer, R. A. Steeman, H. B. Brom, L. J. De Jongh, M. Fujita, and K. Machida, *Physica B+C* **145**, 299 (1987).
- [28] J. C. Bonner and M. E. Fisher, *Phys. Rev.* **135**, A640 (1964).
- [29] R. B. Griffiths, *Phys. Rev.* **133**, A768 (1964).
- [30] J. H. Barrett, *Phys. Rev.* **86**, 118 (1952).
- [31] K. A. Müller and H. Burkard, *Phys. Rev. B* **19**, 3593 (1979).
- [32] M. Shimozawa, K. Hashimoto, A. Ueda, Y. Suzuki, K. Sugii, S. Yamada, Y. Imai, R. Kobayashi, K. Itoh, S. Iguchi, M. Naka, S. Ishihara, H. Mori, T. Sasaki, and M. Yamashita, *Nat. Commun.* **8**, 1821 (2017).
- [33] N. Das and S. G. Mishra, *J. Phys.: Condens. Matter* **21**, 095901 (2009).
- [34] S. Rowley, L. J. Spalek, R. P. Smith, M. P. M. Dean, M. Itoh, J. F. Scott, G. G. Lonzarich, and S. S. Saxena, *Nat. Phys.* **10**, 367 (2014).
- [35] Y. P. Varshni, *Phys. Rev. B* **2**, 3952 (1970).
- [36] The relatively higher transition temperature detected here is due to the higher measurement frequency (32 MHz) compared to the frequency for other measurements. The frequency dependence is evident in the permittivity measurement.
- [37] M. Poirier, M. Castonguay, A. Revcolevschi, and G. Dhalenne, *Phys. Rev. B* **52**, 16058 (1995).
- [38] S. Horiuchi, Y. Okimoto, R. Kumai, and Y. Tokura, *Science* **299**, 229 (2003).
- [39] K. S. Cole and R. H. Cole, *J. Chem. Phys.* **9**, 341 (1941).
- [40] P. Lunkenheimer, S. Kastner, M. Köhler, and A. Loidl, *Phys. Rev. E* **81**, 051504 (2010).
- [41] J. Brooke, T. F. Rosenbaum, and G. Aeppli, *Nature (London)* **413**, 610 (2001).
- [42] B. Champagne, E. Deumens, and Y. Öhrn, *J. Chem. Phys.* **107**, 5433 (1997).